Research on Rotor Position Detection Method of Printed PMSM Based on Leakage Magnetic Field of Rotor

Xianming Deng [1], Junhong Zhou [1], Lei Hao [1], Zhihua Fan [1], and Na Liu [2]

[1] Jiangsu Province Laboratory of Mining Electric and Automation, China University of Mining and Technology
Xuzhou, 221116, China

[2] Aerospace Information Research Institute, Chinese Academy of Sciences
Suzhou, 215000, China
xmdengcumt@126.com, Junhongzhou@cumt.edu.cn

Abstract ─ With the merits of simple structure, strong stability and high power factor, the application of Permanent Magnet Synchronous Motor (PMSM) have become more and more widespread. Meanwhile, rotor position information of PMSM is of vital importance to motor driving. This paper is mainly to research the rotor position detection of Printed PMSM, and, by applying fluxgate technology into the detection process, the rotor position is determined based on the leakage magnetic field of the rotor. The simulation of the rotor leakage magnetic field is made using Finite Element Analysis (FEA), which verifies the feasibility of rotor position detection methods based on the Leakage Magnetic Field of Rotor. Finally, through the experimental prototype of Printed PMSM and fluxgate sensor, Printed PMSM can be driven using a rotor position detected by fluxgate sensors. Fluxgate sensors have advantages of high resolution, strong anti-interference ability, good stability, wide measurement range and ability of miniaturization design, making it suitable to detect weak leakage magnetic field at the end of the rotor so that Printed PMSM has advantages of integration and easy maintenance. Meanwhile, methods mentioned in this paper/article are also applicable to other kinds of PMSM and have certain guiding significance for the integration design of PMSM.

Index Terms ─ Finite Element Analysis (FEA), leakage magnetic field of rotor, printed PMSM, rotor position information.

I. INTRODUCTION

In recent years PMSM has received a lot of researches and is widely used in various fields, which has become mainstream of AC speed regulation and servo field [1]. In the closed-loop control system of PMSM, motor rotor position is an indispensable physical quantity for PMSM control. A lot of researches on sensor-less detection technology have been done, but due to its high requirements to motor, it is difficult to accurately control motor under low speed and zero speed. In addition, the control algorithm is complex, which cannot guarantee the accuracy of rotor position estimation [2-3], so position sensors are still irreplaceable in high performance PMSM control systems. Furthermore, PMSM has the advantage of high power-density and its volume is gradually becoming smaller, so additional position sensors are becoming design burdens, resulting in new design that is more likely to integrate position sensor built-in.

Printed PMSM belongs to disk type motor and has merits of short axial distance, simple structure, mature production process, convenient, low cost, small mechanical tolerance. It has great advantage in large-scale applications, and is mainly applied to aerospace, computer peripherals, power tools, electric vehicles, etc. where the requirements for wheelbase are high. For Printed PMSM, this paper proposes a rotor position detection method based on leakage magnetic field, which has better linearity and precision than traditional Hall method.

II. ANALYSIS OF STRUCTURE AND CONTROL TECHNOLOGY

A. Structure of Printed motor

Figure 1 (a) shows the Printed PMSM structure, including rotor, magnetic conductive plate and Printed armature winding [4]. Rotor is composed of a permanent magnet and a stator core. Magnetic steel is magnetized axially and is laid on rotor core. The adjacent magnetic steels are opposite in magnetic polarity, and N poles and S poles are arranged alternately. There are many choices for the shape of magnetic steel: cylindrical, fan-shaped and trapezoidal. Printed windings are applied to stator, and stator windings are fixed on magnetic conductive plate which only functions to constitute a good magnetic loop. The ideal structure of rotor permanent magnet is fan-shaped, but this kind of structure has high cost.

Submitted On: October 27, 2019
Accepted On: January 20, 2020

Therefore, the laboratory designed rotor permanent magnet of the motor adopts a cylindrical structure, as shown in Fig. 1 (b). The prototype of motor designed in laboratory is shown in Fig. 1 (c).

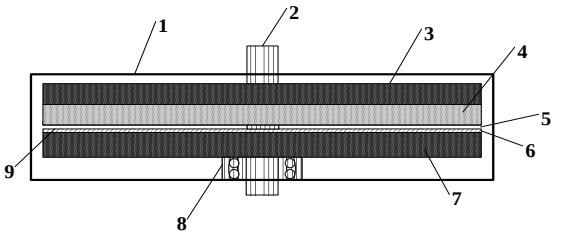

(a)

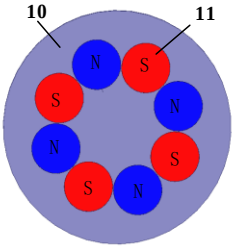

(b)

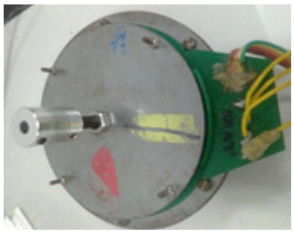

(c)

1-Casing, 2-Shaft, 3-Rotor core, 4-Permanent magnet, 5-Air gap, 6-PCB winding, 7-Stator core, 8-Bearing, 9-Insulating paper, 10-rotor core, 11- Permanent magnet

Fig. 1. (a) Structure of Printed PMSM, (b) rotor structure, and (c) prototype of Printed PMSM.

The conventional Printed PMSM stator adopts a spiral winding structure, as shown in Fig. 2 (a). The winding conducting bar of this structure are compact and three-phase windings are distributed in each layer, so the utilization rate of Printed board is relatively high. The endline is long, and copper loss is high. Stator of Printed PMSM designed by laboratory adopts wave windings structure, as shown in Fig. 2 (b). Compared with spiral winding, Printed circuit board with wave winding structure has a very high utilization rate, and the number of via holes per phase winding is small. Besides, the structure of wave winding is simpler than that of spiral winding. Moreover, at the same speed, the induced electromotive force of wave winding is larger. The parameters of Printed PMSM designed by laboratory are shown in Table 1.

(a)

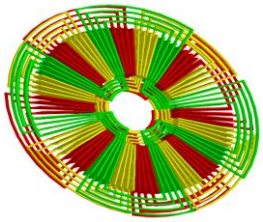

(b)

Fig. 2. (a) Spiral winding and (b) wave winding.

Table 1: Main parameters of Printed PMSM

Parameters	**Value**
Rated power/W	48
Rated voltage/V	5
Rated current/A	4
Rated Torque/ Nm	0.5
Phase number	3
PCB layer number	6
Number of turns per phase	4
Number of poles	4
Rated speed/rpm	750
Diameter of permanent magnet/mm	25
Thickness of permanent magnet/mm	4
Flux linkage/Wb	0.023
Stator diameter/mm	120
Stator resistance/Ω	0.5
Air gap/mm	4
Conducting bar thickness/mm	0.2
Conducting bar width/mm	0.8
Maximum current/A	6
Maximum voltage/V	12

B. Mathematical model of Printed PMSM

The mathematical model of Printed PMSM is the same as that of conventional PMSM. In order to simplify the mathematical model of a Printed PMSM, changing the reference coordinate system is often required. For control system, although the actual parameter is a sinusoid, we still want the system variable to be simple. Therefore, it is possible to convert the sinusoidal quantity to DC quantity by establishing a reference coordinate system whose rotation speed is consistent with the angular velocity of sinusoidal variable, which is called Park transformation in mathematics. The system can be decoupled with Clark and Park transformation performed on motor mathematical equation in ABC stationary coordinate system. The specific equations are as follows.

Clark transformation and its inverse transformation:

$$C_{3s/2s}=\frac{2}{3}\begin{bmatrix}1 & -\frac{1}{2} & -\frac{1}{2}\\ 0 & \frac{\sqrt{3}}{2} & -\frac{\sqrt{3}}{2}\end{bmatrix}, \tag{1}$$

$$C_{2s/3s}=\frac{2}{3}\begin{bmatrix}1 & 0\\ -\frac{1}{2} & \frac{\sqrt{3}}{2}\\ -\frac{1}{2} & -\frac{\sqrt{3}}{2}\end{bmatrix}. \tag{2}$$

Park transformation and its inverse transformation:

$$C_{2s/2r}=\begin{bmatrix}\cos\theta & \sin\theta\\ -\sin\theta & \cos\theta\end{bmatrix}, \tag{3}$$

$$C_{2r/2s}=\begin{bmatrix}\cos\theta & -\sin\theta\\ \sin\theta & \cos\theta\end{bmatrix}. \tag{4}$$

The mathematical model of transformed PMSM in d-q rotating coordinate system is:

$$\begin{cases} u_{\mathrm{d}} = \mathrm{R}_{\mathrm{s}} i_{\mathrm{d}} + p\psi_{\mathrm{d}} - \omega\psi_{\mathrm{q}} \\ u_{\mathrm{q}} = \mathrm{R}_{\mathrm{s}} i_{\mathrm{q}} + p\psi_{\mathrm{q}} + \omega\psi_{\mathrm{d}} \end{cases}, \tag{5}$$

$$\begin{cases} \psi_{\mathrm{d}} = L_{\mathrm{d}} i_{\mathrm{d}} + \psi_{\mathrm{f}} \\ \psi_{\mathrm{q}} = L_{\mathrm{q}} i_{\mathrm{q}} \end{cases}. \tag{6}$$

where u_{d} and u_{q} are respectively the stator voltage component of d and q axis, id and i_{q} are respectively the stator current component of d and q axis, ψ_{d} and ψ_{q} are respectively the main flux component of d and q axis, L_{d} and L_{q} are respectively the inductance of d and q axis, ψ_{f} is flux produced by permanent magnet.

The torque expression of motor is:

$$T_{\mathrm{e}} = 1.5 n_{\mathrm{p}} [\psi_{\mathrm{f}} i_{\mathrm{q}} + (L_{\mathrm{d}} - L_{\mathrm{q}}) i_{\mathrm{d}} i_{\mathrm{q}}]. \tag{7}$$

Since L_{d} and L_{q} are equal in Printed PMSM, equation (7) can be simplified as:

$$T_{\mathrm{e}} = 1.5 n_{\mathrm{p}} \psi_{\mathrm{f}} i_{\mathrm{q}}. \tag{8}$$

C. Control technology of Printed PMSM

Printed PMSM can be controlled by vector control technology. Vector control is also called field oriented control or decoupling control. The principle of rotor-oriented vector control is to transform the motor model from a stationary coordinate system into a rotating coordinate system, and a model similar to a DC machine can be obtained. By controlling stator excitation input, the torque and flux can be separately controlled to achieve torque control.

According to the torque equation (7), the output torque of motor can be controlled by controlling stator current i_{q}. Since the L_{d} and L_{q} are equal in Printed PMSM, i_{d}=0 control is the maximum torque/current ratio control, that is to say, maximum torque output can be obtained with same bus current. Figure 3 shows the i_{d}=0 control vector diagram.

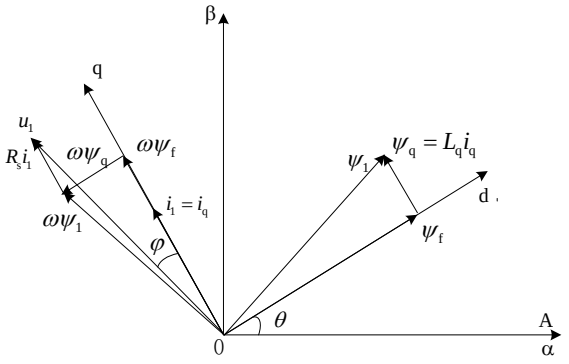

Fig. 3. i_{d}=0 control vector diagram.

Figure 4 shows a control block diagram of id=0 vector control of Printed PMSM. In the figure, θ and n are respectively the rotor position angle and motor speed; i_{a}, i_{b} , i_{c} are three-phase instantaneous currents; id and i_{q} are respectively d and q axis stator current components. The inner loop of system is current loop, and current regulator outputs the reference value of space voltage vector. The outer loop of system is speed loop, and speed regulator outputs the given current. The difference between set value of current and actual value is input to current regulator. The output reference vector of current regulator is sent to the inverter to generate a PWM signal to control inverter power tube, thereby realizing the control of stator current of Printed PMSM. Therefore, rotor position is still important for driving Printed PMSM.

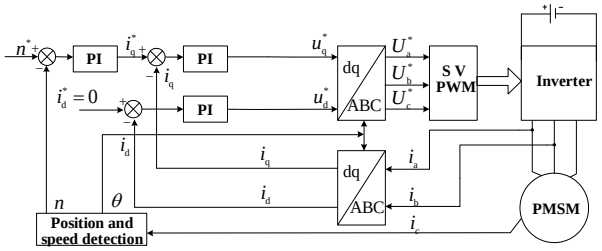

Fig. 4. i_{d}=0 control system block diagram.

III. FEA OF PRINTED PMSM LEAKAGE MAGNETIC FIELD

The direction of the air gap magnetic flux density of Printed PMSM designed by laboratory is axial, so the magnetization direction of permanent magnet is axial, and the main simulation parameters of Printed PMSM are shown in Table 2. The magnetic field generated by permanent magnet passes axially through the air gap, and back to the air gap to the opposite polarity permanent magnet through the stator magnetic plate. However, due to the scattering of magnetic field of permanent magnet, there is leakage magnetic flux directly closed in the air gap at the radial edge of permanent magnet. The simulation model of motor established in the finite element software Ansoft Maxwell is shown in Fig. 5 (a), and for better observation, the rotor core is hidden [5]. When motor is under no-load condition, the magnetic flux density distribution at the radial edge of rotor permanent magnet in which the radius r = 47mm is shown in Fig. 5 (b), and the magnetic flux density distribution and magnetic flux density harmonic histogram in radial direction of this radius are shown in Fig. 5 (c) and Fig. 5 (d), respectively. It can be seen from Fig. 5 (b) that the magnetic field is diverging around the circumference of rotor permanent magnet edge, and the magnetic field of the opposite polarity is reversed. According to the Fig. 5 (c), the radial magnetic field distribution at this circumference is approximately sinusoidal. Since there are 4 pairs of poles in this motor, the number of magnetic field cycles is 4 in one mechanical cycle. By performing harmonic analysis on the magnetic flux density of Fig. 5 (c), result is obtained

which is shown in Fig. 5 (d). It can be seen that except for the fundamental wave, the third harmonic is the highest, and the other harmonic content is very small. Therefore, the third harmonic is the main factor causing distortion of the magnetic field distribution.

Table 2: Main simulation parameters of Printed PMSM

Parameters	**Value**
Rated power/W	36
Phase number	3
PCB layer number	6
Number of turns per phase	4
Number of poles	4
Maximum speed/rpm	2000
Thickness of permanent magnet/mm	4
Outer diameter of PM/mm	92
Inner diameter of PM/mm	40
Air gap/mm	4
Conducting bar thickness/mm	0.2
Conducting bar width/mm	0.8

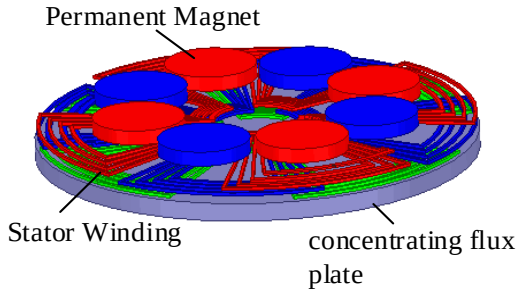

(a)

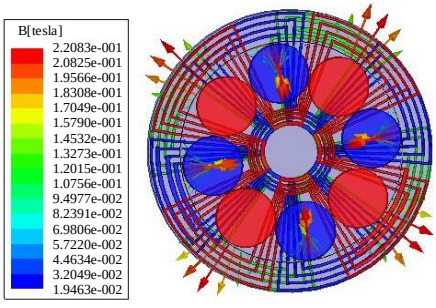

(b)

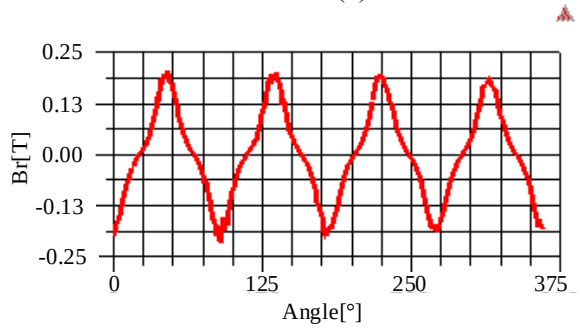

(c)

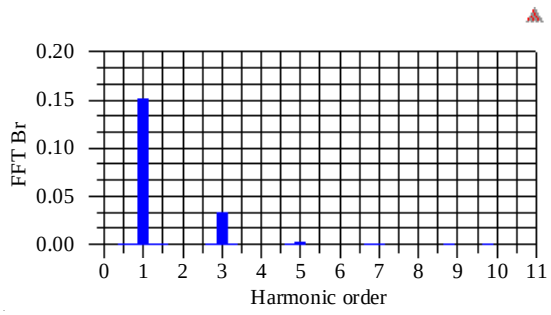

(d)

Fig. 5. (a) Motor simulation model with hidden rotor core, (b) magnetic flux density distribution (r=47mm), (c) magnetic flux density distribution (r=47mm), and (d) magnetic flux density harmonic histogram (r=47mm).

The magnetic field distribution vector at the circumference of radius r = 60mm (the circumference of motor stator edge) is shown in Fig. 6 (a). The magnetic flux density distribution and magnetic flux density harmonic histogram at the radial direction of this circumferential are shown in Fig. 6 (b) and Fig. 6 (c). It can be concluded that the magnetic field at this circumference is substantially sinusoidal in space, and magnetic field starts from the N pole of permanent magnet and returns to the S pole along the air gap in radial direction. In this case, the third harmonic content of radial magnetic field is also higher than other harmonic content, but significantly less than the third harmonic content in the simulation of Fig. 5.

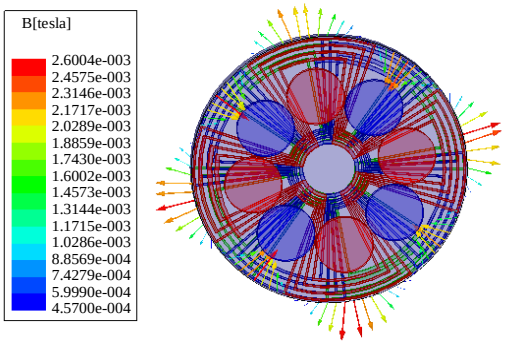

(a)

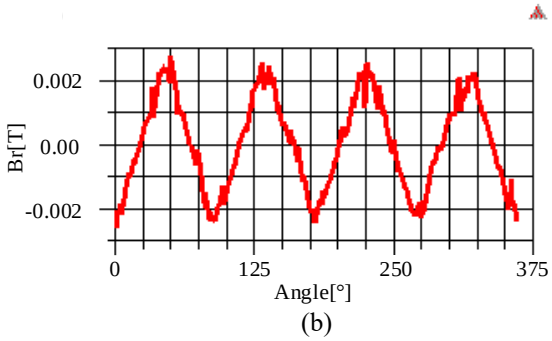

(b)

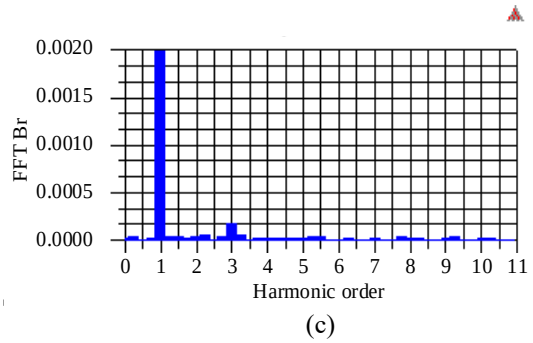

(c)

Fig. 6. (a) Magnetic flux density distribution (r=60mm), (b) magnetic flux density distribution (r=60mm), and (c) magnetic flux density harmonic histogram (r=60mm).

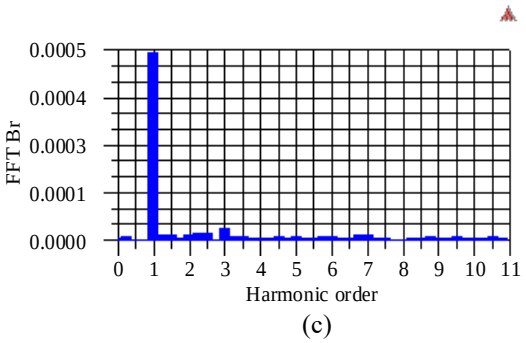

(c)

Fig. 7. (a) Magnetic flux density distribution (r=65mm), (b) magnetic flux density distribution (r=65mm), and (c) magnetic flux density harmonic histogram (r=65mm).

At the circumference of r = 60mm, the vector diagram of magnetic field distribution is shown in Fig. 7 (a), the magnetic flux density distribution and magnetic flux density harmonic histogram in the radial direction of this circumference are shown in Figs. 7 (b) and (c), respectively.

From the simulation, it can be seen that the magnetic field harmonic in this case is slightly more than that in the simulation of Fig. 6, and the magnetic flux density is about 500μT. Therefore, two fluxgate detectors can be mounted on the circumference of the air gap between the stator and rotor of motor with a radius r = 65 mm, that is, a circumference of 5 mm from the edge of stator.

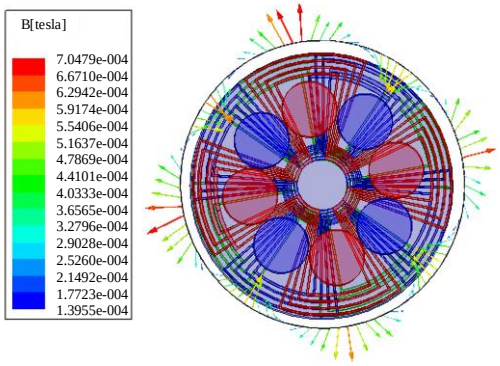

(a)

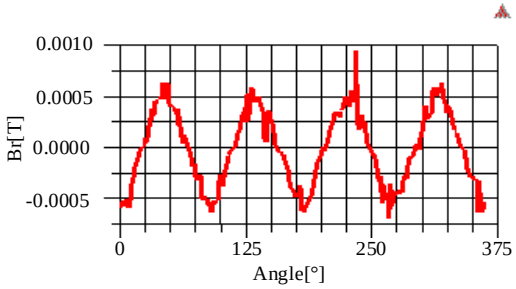

(b)

The above simulations are all carried out under no-load condition of the motor. When motor is running under rated state, stator current will generate stator magnetic field. In this case, the magnetic flux density distribution and the harmonic histogram in the radial direction at the circumference of radius r = 65 mm are as shown in Figs. 8 (a) and 8 (b), respectively. It can be seen that, compared with the magnetic leakage distribution of no-load motor, the symmetry of leakage magnetic flux distribution of each pair of poles is deteriorated because the motor running in rated state is affected by stator magnetic field, and not only leakage magnetic flux amplitudes are different, but also the harmonics are different, which increase the difficulty of leakage magnetic flux detection.o

According to the above simulation analysis, the leakage magnetic flux intensity of permanent magnets is different at different positions, and so is the magnetic field distribution under no-load and rated operating conditions. In no-load mode, on the circumference of the air gap of radius r = 47mm, sinusoidal distribution of magnetic flux density is better, the harmonic law is obvious, and the signal intensity is large. While in rated mode, on the air gap circumference with radius r = 60mm and r = 65mm, the magnetic flux density distribution still has a good sinusoidally degree, but harmonics become more complicated and signal intensity get smaller with the increase of radius. In Printed disc type motor, the radial outer end of permanent magnet is relatively wide, and in general motor, motor end space is also relatively rich, which is a preferred position for installing magnetic sensor.

However, at the end of motor, leakage magnetic flux density of permanent magnet is weak. A generally magnetic sensor cannot detect the magnetic field at this position, so magnetic sensor needs to be installed at a suitable position inside the motor. For example, Hall

sensor has a generally detectable magnetic field intensity range of ± (0.1~0.15) T. According to the above simulation, this leakage flux intensity is inside the motor of this simulation, so installing Hall sensor can be very troublesome and difficult to repair and replace. The fluxgate sensor can detect weak magnetic fields, and its magnetic field detection has a wide range of intensity and high resolution. According to the range of leakage magnetic flux intensity at the end of motor, the requirement of leakage magnetic field intensity detection at this position can be satisfied by rationally designing structure of fluxgate sensor. Therefore, compared with other magnetic sensors, the fluxgate sensor is more suitable for determining the rotor position of motor due to its special performance. Therefore, compared with other magnetic sensors, fluxgate sensor is more suitable for determining the rotor position of motor due to its special performance.

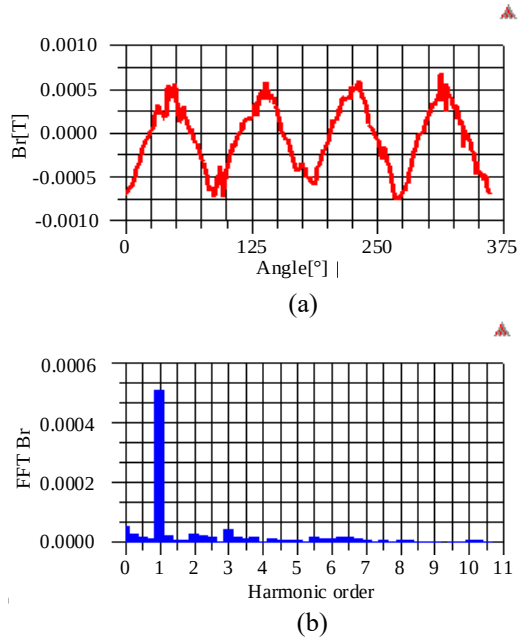

Fig. 8. (a) Magnetic flux density distribution under rated condition (r=65mm), (b) and magnetic flux density harmonic histogram under rated condition (r=65mm).

IV. ROTOR POSITION DETECTION METHOD BASED ON LEAKAGE MAGNETIC FIELD

A. Working principle of fluxgate sensor

The fluxgate sensor is a device sensitive to external magnetic field, which made by utilizing the property that magnetic core material has a nonlinear change in periodic supersaturation state, and is mainly composed of an iron core, an excitation coil and an induction coil. The working principle can be described by Fig. 9.

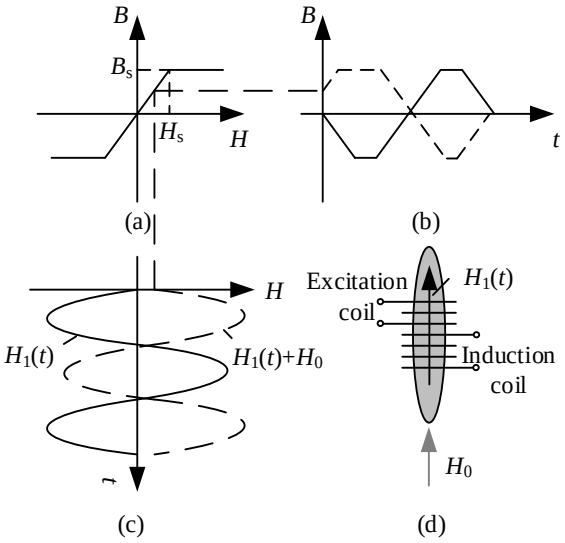

Fig. 9. (a) Magnetization curve of ferromagnetic material, (b) magnetic flux density curve, (c) magnetic field strength curve, and (d) coil structure diagram.

Figure 9 (a) shows the magnetization curve of ferromagnetic material. When the magnetic field intensity $H_1(t)$ generated by excitation coil periodically changes and its amplitude is greater than the saturation magnetic field intensity H_s of core material, core material is in periodic supersaturation state, when the magnetic flux density changes as shown by solid line in Fig. 9 (b). Since the magnetization curve of core material is symmetrical, the magnetic induction signal shown by solid line in Fig. 9 (b) contains only the odd harmonics of magnetic field intensity $H_1(t)$, and the induced voltage of induction coil contains only odd harmonics. When there is an external magnetic field intensity H_0, magnetic field strength changes as shown by dashed line in Fig. 9 (c). The magnetic flux density curve at this time is as shown by broken line in Fig. 9 (b), and the upper half is wider than the lower half, which will cause even harmonics of induced voltage signal of induction coil in Fig. 9 (d). In even harmonic of the signal, because the second harmonic content is proportional to the magnitude of external magnetic field within a certain range of external magnetic field intensity, second harmonic signal is often used to detect the magnitude of external magnetic field intensity H_0 [6].

Second harmonic signal that the single-core flux sensor of single-core core outputs is small, and there are a large number of useless odd harmonic signals, resulting in difficult useful signal extraction. Therefore, a double-core sensor is generally selected. The excitation coil of double-core sensor is wound on two cores in the same polarity and the number of turns of two coils is equal, and induction coil wraps two core windings. When excitation coil applies AC excitation and the core of

sensor reaches a periodic supersaturation state, the odd harmonics in voltage signal induced by induction coil cancel each other, and the even harmonics overlap each other.

B. Mathematical model of fluxgate detection

The fluxgate of double iron core structure can effectively suppress useless signal and increase useful signal. The structure diagram is shown in Fig. 10.

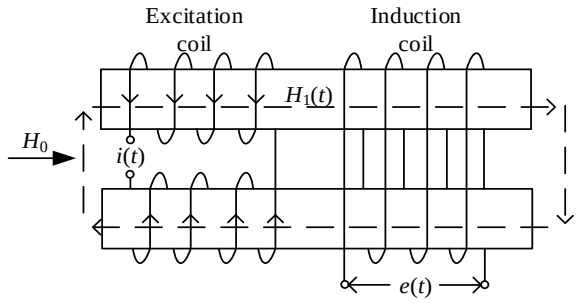

Fig. 10. Structural sketch of dual-core fluxgate.

In Fig. 10, N_1 is the number of excitation coils of two cores, N_2 is the number of turns of induction coil, S is the cross-sectional area of core, and μ is magnetic permeability. The excitation coil is supplied with an alternating current of which the frequency is f_{ex}, which produces the internal magnetic field intensity $H_1(t)$ having equal magnitude and opposite direction on two cores, while iron core is in a periodic supersaturation state. The internal magnetic field intensity $H_1(t)$ can be described by:

$$H_1(t) = H_m \sin(2\pi f_{ex} t), \tag{9}$$

where H_m is the amplitude of internal magnetic field intensity $H_1(t)$.

If there is no external magnetic field, it can be known from Faraday law of electromagnetic induction that the alternating magnetic field in two cores changes the magnitude of the induced voltage generated on induction coil, and the direction is opposite, so the fluxgate sensor has no voltage signal output.

If there is an external magnetic field intensity H_0, the magnetic fields inside two cores are:

$$\begin{cases} H'(t) = H_1(t) + H_0 \\ H''(t) = H_1(t) - H_0 \end{cases}, \tag{10}$$

where $H'(t)$ is the internal magnetic field of one core, and $H''(t)$ is the internal magnetic field of the other core.

The induced voltage on fluxgate sensor induction coil is:

$$e(t) = -N_2 S \frac{d[\mu'(t)H'(t)]}{dt} + N_2 S \frac{d[\mu''(t)H''(t)]}{dt}, \tag{11}$$

where $\mu'(t)$ and $\mu''(t)$ are the magnetic permeability functions of two cores, respectively. The direction of magnetic field generated by excitation signal is periodically changed, but magnetic permeability has no polarity, that is, the excitation of magnetic field in both directions produces two changes in magnetic permeability. Therefore, the frequency of magnetic permeability change is twice that of the magnetic field, which is an even function in time. Equation (12) shows the magnetic permeability expanded according to the Fourier series:

$$\begin{aligned} \mu(t) &= \mu_{0m} + \mu_{2m} \cos 4\pi f_{ex} t + \mu_{4m} \cos 8\pi f_{ex} t + \ldots \\ &= \sum_{n=0}^{\infty} \mu_{2n\times m} \cos 4n\pi f_{ex} t. \end{aligned} \tag{12}$$

Because of the existence of external magnetic field, the saturation and magnetic permeability of two cores are different. By substituting equations (9), (10), (12) into equation (11), it can be concluded that:

$$\begin{aligned} e(t) = -N_2 S H_m [& 2\pi f_{ex} \Big(\sum_{n=0}^{\infty} \mu'_{2n\times m} \cos 4n\pi f_{ex} t \cdot \sin 2\pi f_{ex} t \\ & - \sum_{n=0}^{\infty} \mu''_{2n\times m} \cos 4n\pi f_{ex} t \cdot \sin 2\pi f_{ex} t\Big) \\ & - \cos 2\pi f_{ex} t \cdot \Big(\sum_{n=0}^{\infty} 4n\pi f_{ex} \mu'_{2n\times m} \sin 4n\pi f_{ex} \\ & - \sum_{n=0}^{\infty} 4n\pi f_{ex} \mu''_{2n\times m} \sin 4n\pi f_{ex}\Big)] \\ & + N_2 S H_0 f_{ex} \sum_{n=0}^{\infty} 4n\pi \mu'_{2n\times m} \sin 4n\pi f_{ex} \\ & + N_2 S H_0 f_{ex} \sum_{n=0}^{\infty} 4n\pi \mu''_{2n\times m} \sin 4n\pi f_{ex}, \end{aligned} \tag{13}$$

where $\mu'_{2n\times m}$ and $\mu''_{2n\times m}$ are the Fourier decomposition coefficients of magnetic permeability of two cores. Generally, the strength of external magnetic field detected by fluxgate sensor is much smaller than the saturation magnetic field of iron core, so the difference of the total magnetic field after superimposing external magnetic field in two cores is small, that is, the difference in magnetic permeability between two cores is small. In order to simplify the analysis, assuming that changes in the magnetic permeability of two cores are both $\mu(t)$, then equation (13) can be simplified as:

$$e(t) = 2N_2 S H_0 f_{ex} \sum_{n=0}^{\infty} 4n\pi \mu_{2n\times m} \sin 4n\pi f_{ex}. \tag{14}$$

Comparing equation (14) with equation (13), it can be seen that in double core structure, voltage signals independent of the external magnetic field are mutually suppressed, and the related voltage signals are superimposed on each other, thereby effectively reducing the difficulty of extracting useful signals.

C. Advantages of fluxgate sensor

A comparison of three common commercial position sensors is shown in Table 3.

Table 3: Comparison of three position sensors

	Photoelectric Encoder	Resolver	Hall Sensor
Volume	Little small	Large	Small
Structure	Simple	Complicate	Simple
Resolution	High	Little high	Low
Precision	High	Little high	Low
Range of operation	Small	Large	Small
Temperature	High	Low	High
Speed range	High	Low	High
Request to working environment	High	Low	Low
Cost	High	Little high	low

The fluxgate sensor is a magnetic sensor capable of detecting a weak magnetic field, of which the basic structure is composed of an iron core, an induction coil and excitation coil wound around iron core, and belongs to an induction transformer structure. When fluxgate sensor is working, it is necessary to apply an alternating current power to its excitation coil to make the core of fluxgate in a state of periodic supersaturation. When there exist an external magnetic field, the induction coil of fluxgate will induce an electromotive force related to the strength of external magnetic field. Fluxgate sensor has the advantages of high resolution, strong anti-interference ability, good stability, wide measurement range, and ability of miniaturized design [7-11], making it can be designed as a sensor to detect the position of PMSM rotor.

D. Analysis of detection method based on leakage magnetic field of rotor

The detection method based on leakage magnetic field of rotor is simple in structure and can be integrated with motor. However, this method has high requirements on design, manufacture and control of motor, and its accuracy is also affected by motor operating conditions. In the case where the position of motor space is strictly required, the volume and mounting position of fluxgate sensor must also be considered [12]. This section will analyze the effects of motor system on rotor position detection.

a) Leakage flux distribution under the influence of working conditions

According to the analysis of Printed permanent magnet synchronous motor, the magnetic field distribution on the circumference of the radius r = 65 mm at the air gap between stator and motor rotor is approximately sinusoidal under no-load conditions, and leakage flux distribution of each pair is similar. However, when motor is running under rated conditions, it can be seen from Fig. 8 (a) that the leakage magnetic flux distribution of each pair of poles changes and is no longer the same. However, when motor is running under rated conditions, it can be seen from Fig. 8 (a) that the leakage magnetic flux distribution of each pair of poles changes and is no longer the same. Influenced by stator magnetic field, compared with Fig. 7 (b), the leakage flux distribution of four pairs of poles in Fig. 8 (a) is different, and the amplitude of magnetic field intensity is obviously asymmetrical. It can be seen that the leakage flux distribution of motor is affected by operating conditions of the motor, which affects the accuracy of rotor position detection of motor.

b) Leakage flux distribution under the influence of rotor permanent magnet migration

The motor model designed by laboratory is little rough. During the manufacturing process, the installation of permanent magnet will be inevitably deviated, that is, center positions of permanent magnets are not on one circumference. Taking no-load operation of motor as an example, the simulation analyzes distribution of leakage magnetic flux when permanent magnet is deviated. Taking two permanent magnets on the same diameter as an example, the permanent magnets of motor simulation model are offset, that is, one permanent magnet is shifted inward by 1 mm, and one permanent magnet is shifted outward by 1 mm, as shown in Fig. 11(a). The magnetic flux density distribution in radial direction on the circumference of radius r = 65 mm at the air gap between stator and rotor of motor is as shown in Fig. 11 (b). It can be seen that the leakage magnetic flux distribution of four pairs of poles is significantly different, and the amplitude is no longer symmetrical. By analyzing harmonic of leakage magnetic flux, the magnetic flux density harmonic histogram is obtained in Fig. 11 (c), and harmonic content is significantly increased. This is the result of the migration of two permanent magnets. During the motor manufacturing process, there may be cases where centers of eight permanent magnets are all offset. The distortion of leakage magnetic flux caused by permanent magnet migration significantly increases the error of motor rotor position detection.

According to the above analysis, the magnetic flux detection method includes the detection error of fluxgate sensor itself, and also has additional detection error caused by motor system. Since the motor is a four-pole structure, the leakage magnetic flux distribution of each pair is easily affected by motor manufacturing and operation conditions, so that the leakage magnetic flux distribution of four pairs of poles is different, which increases the difficulty of detecting rotor position of motor.

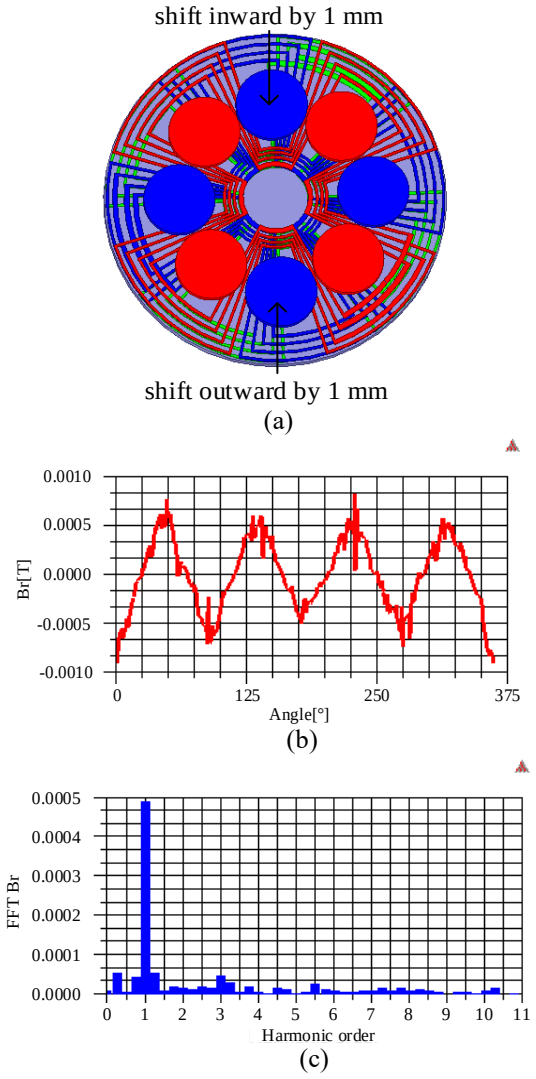

Fig. 11. (a) Permanent magnet shift diagram (r=65mm), (b) magnetic flux density distribution with shifted permanent magnet (r=65mm), and (c) magnetic flux density harmonic histogram with shifted permanent magnet (r=65mm).

V. PROTOTYPE EXPERIMENT ANALYSIS

A. Production and testing of fluxgate sensors

According to the principle of fluxgate, fluxgate sensor core needs to use a soft magnetic material with a small coercive force. However, in the sensor structure designed herein, the strip 1J85 does not have sufficient physical support capability, so it is necessary to design a skeleton support material. The core skeleton model designed by Soildworks software is shown in Fig. 12 (a).The core material 1J85 is cut and then attached to the groove of core frame and fixed with glue. Its physical picture is shown in Fig. 12 (b). The excitation coil is wound directly on both sides of core frame. In order to facilitate the winding of induction coil, induction coil winding skeleton is designed, and model and physical map are respectively shown in Figs. 12 (c) and (d).

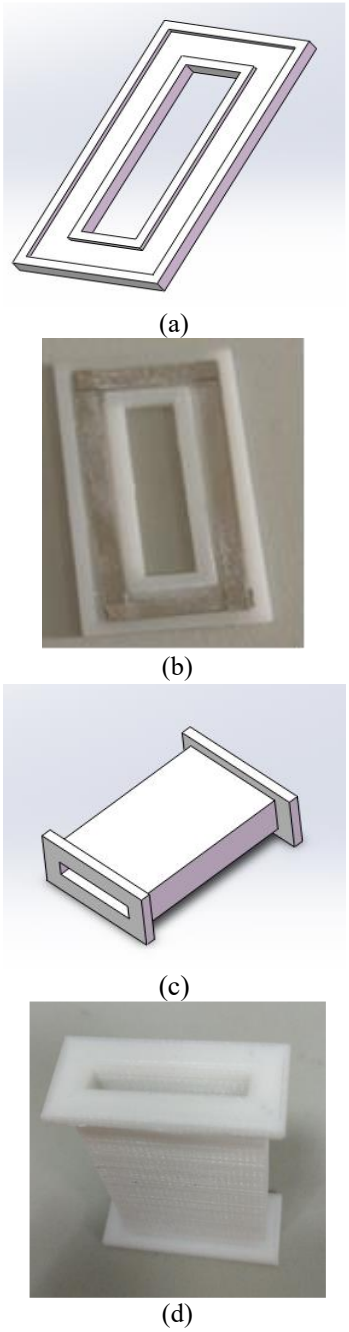

Fig. 12. (a) Core skeleton model, (b) core skeleton actual picture, (c) induction coil winding skeleton model, and (d) induction coil winding skeleton actual picture.

Induction coil winding skeleton and iron core skeleton are matched structures, and iron core skeleton can be inserted into the groove of induction coil winding skeleton. Induction coil winding skeleton total length is 35mm, width is 25mm, and wall thickness is 2mm. In

order to enable core skeleton after winding excitation coil to be inserted into the rectangular groove of induction coil winding skeleton, the designed rectangular groove has a certain margin, of which the length is 17.5 mm and width is 3 mm. Both the core skeleton and induction coil winding skeleton are Printed by a 3D printer, and printing consuming materials are made of PLA (polylactic acid) material having good mechanical and physical properties.

After skeleton model is designed, the excitation coil and induction coil need to be wound on skeleton. The total turns of excitation coil is 110, and copper enameled wire with a diameter of 0.29mm is selected. The total turns of induction coil is 400. For easy winding, a copper enameled wire with a diameter of 0.2 mm is selected. The number of turns of excitation coil and induction coil can be adjusted according to the actual situation, and the physical diagram of fluxgate detector is shown in Fig. 13.

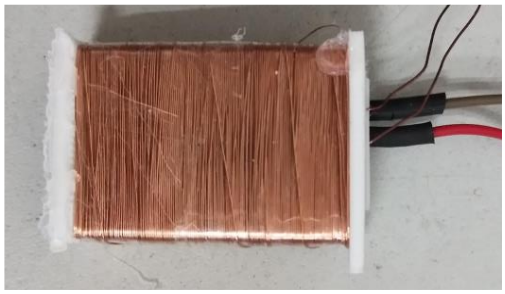

Fig. 13. Fluxgatae detector actual picture.

B. Rotor position detection of Printed PMSM

Position detection method based on rotor leakage flux is based on a laboratory-designed Printed PMSM. The main magnetic flux direction of motor is axial, and leakage magnetic flux direction of rotor permanent magnet is almost radial. It can be seen from Fig. 6 that the radial magnetic field strength at the circumference of motor stator is about 0.002T, and the magnetic field intensity exceeds designed detection range of fluxgate detector. Therefore, fluxgate detector needs to be installed at a circumference larger than stator radius. Two fluxgate detectors are tangentially placed on the stator of Printed PMSM, as shown in Fig. 14. The motor is a four-pole motor, so two fluxgate detectors are placed with an angular difference of 22.5°. It can be seen that two fluxgate detectors are placed at the end of motor, which is convenient for installation and maintenance, and does not affect the internal structure of motor.

The Printed PMSM designed by laboratory is rough, the air gap length is about 1cm, and this is too large, resulting in uneven air gap. There are only 4 turns per phase winding in motor stator and no stator core. So, the inductance is very small, about 7.8μH, which is difficult to control. In order to facilitate the control, a 1.5mH compensation inductor is connected to each three-phase stator winding of motor in the experiment.

Fig. 14. Installation position of fluxgate detector.

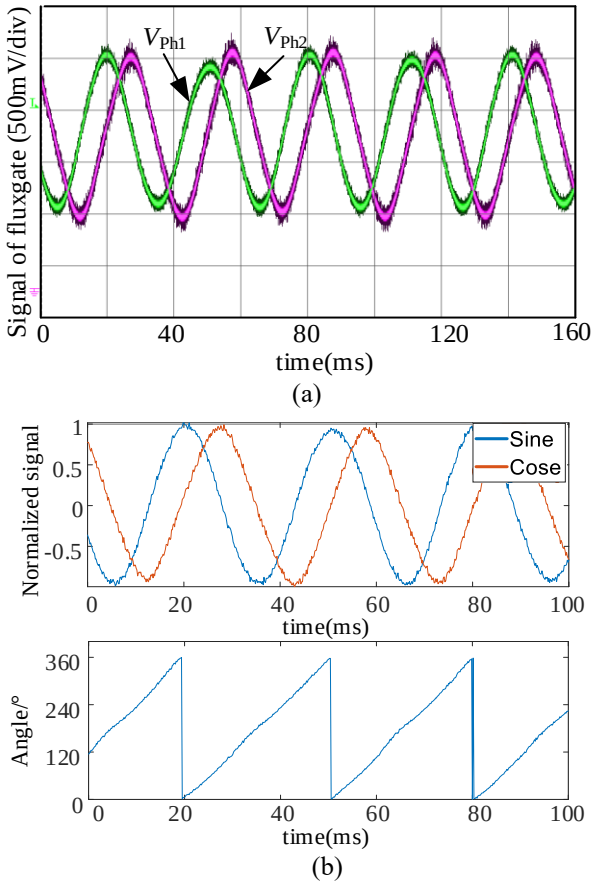

Fig. 15. (a) Output waveform of fluxgate hardware circuit, and (b) angle solving.

When motor is in driving mode and its speed is 500 rpm, waveforms of fluxgate hardware circuit output

signals V_{Ph1} and V_{Ph2} are as shown in Fig. 15 (a). In a mechanical angular cycle, the amplitudes of V_{Ph1} and V_{Ph2} are deviated because the eight rotor permanent magnets of motor have a certain positional deviation during installation, resulting in a difference in flux leakage distribution of four pairs of permanent magnets. Save oscilloscope data and perform signal processing in MATLAB. Then normalize the amplitude of signal and remove DC offset, and solve angle using atan2 function. The result is shown in Fig. 15 (b). Motor is in driving mode, and stator winding is open, and there is no influence of stator current. In this case, fluxgate sensor can accurately identify the rotor position of motor by detecting leakage flux of permanent magnet of motor, and the linearity of angle waveform is good. The motor rotor position detected by leakage flux detection method is an electrical angle. When speed is 500 rpm, the frequency of magnetic field change is four times that of motor rotation.

Using VF control to start Printed PMSM with no load, Phase A current i_A of motor in no-load start-up process and the operation state are shown in Figs. 16 (b) and (c), respectively. No-load start-up current of motor is about 2.8A. The current amplitude after operation state is about 1A, and the current waveform is distorted. Due to the fact that motor production is rough, the air gap of motor is too large and uneven, and harmonics are large, which causes the current to be distorted.

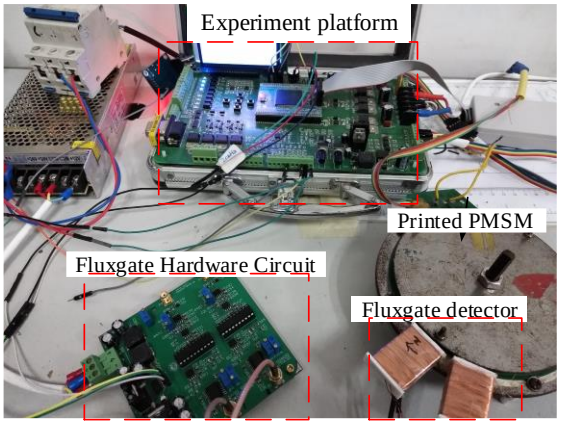

(a)

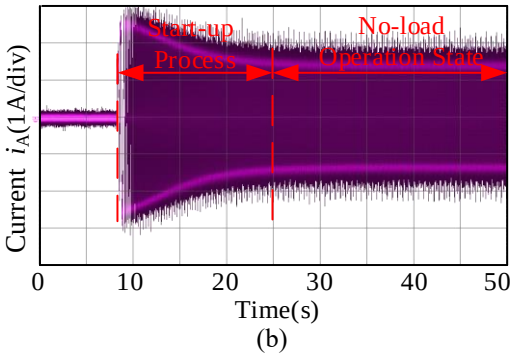

(b)

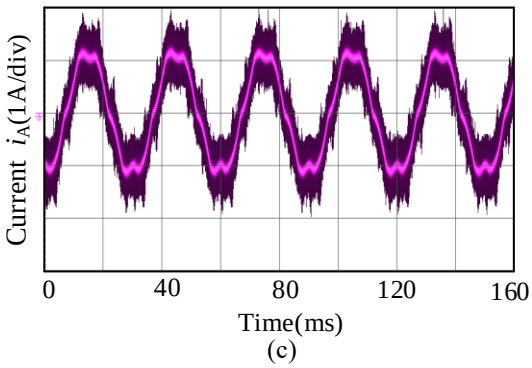

(c)

Fig. 16. (a) Experiment platform, (b) Phase A motor current during VF no-load start-up, and (c) Phase A current in no-load motor.

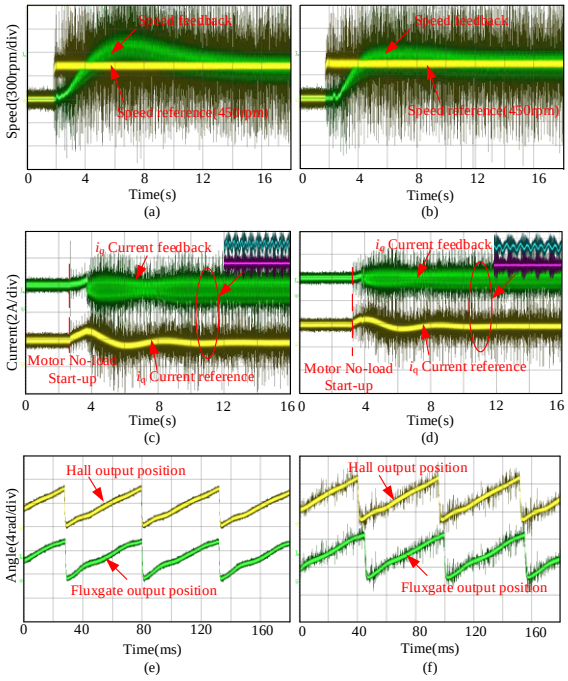

Fig. 17. (a) Motor speed based on Hall sensor, (b) motor speed based on fluxgate sensor, (c) i_q reference and feedback based on Hall control, (d) i_q reference and feedback based on fluxgate control, (e) output position based on Hall control, and (f) output position based on Hall control.

According to the above analysis, the Printed motor laboratory designed causes distortion of current due to manufacturing problems, and motor vibration and torque ripple is large during operation. During the start-up process of motor, the presence of starting current will inevitably affect leakage flux distribution of rotor permanent magnet, thus increasing the difficulty of leakage flux detection. This section still takes id=0 motor

control experiment as an example. Motor is given a speed of 450 rpm and runs at no-load. The motor control experiment waveform based on Hall sensor and fluxgate sensor is shown in Fig. 17. It can be seen from Figs. 17 (a) and (b) that in two sets of experiments, when motor is in steady operation, speed feedback can track the given speed well. Comparing Figs. 17 (e) and (f), in the two sets of experiments, the linearity difference of output angle waveform of fluxgate sensor is smaller than that of Hall sensor. The reason is that manmade sensor is rough, but it has the equivalent performance of a mature Hall sensor. If fluxgate sensor is precision-produced, its performance will exceed Hall sensor.

VI. CONCLUSION

In this paper, the structural characteristics of Printed PMSM are briefly introduced. At the same time, the basic control method and relevant parameters of PMSM used in the experiment are given. In addition, in order to verify the feasibility of detecting rotor position of Printed PMSM based on leakage flux detection, this paper simulates leakage flux distribution around the air gap of Printed PMSM with different radius. The simulation results show that the larger the radius, the smaller leakage magnetic flux and the more complex harmonics is. But fundamental frequency content is always high, that is, the sinusoidally degree is good, which means it is suitable for rotor position detection. In order to detect the weak rotor leakage flux, this paper introduces fluxgate technology, compares the advantages and disadvantages of existing position sensors, and analyzes the influence of motor system error on rotor position detection. Finally, the fluxgate position sensor is designed and fabricated, and it is used to drive Printed PMSM. Feasibility of the method described in this paper is verified by finishing the experiment using this sensor to drive Printed PMSM. The rotor position detection method proposed in this paper is based on the example of Printed PMSM, but it is also applicable to rotor position detection of most traditional PMSM, which means it has good reference value for integrated design of PMSM.

ACKNOWLEDGMENT

This work has been supported by the Postgraduate Research & Practice Innovation Program of Jiangsu Province (KYCX19_2191), Postgraduate Research & Practice Innovation Program of China University of Mining and Technology (ZGKD19_2191) and Natural Science Foundation of Jiangsu Province Grant No. BK20190634.

REFERENCES

[1] Q. N. Ni, M. Yang, X. Dong, X. S. Liu, and D. G. Xu, “State estimation error suppression for PMSM speed observer based on Hall position sensor,” *Transactions of China Electrotechnical Society*, vol. 32, no. 17, pp. 189-198, Sep. 2017.

[2] J. Zhu, L. L. Han, and X. D. Wang, “Status and trends of sensorless control algorithm for PMSM,” *Micromotors*, vol. 46, no. 9, pp. 11-16, Sep. 2013.

[3] J. L. Liu, F. Xiao, Y. Shen, Z. Q. Mai, and C. R. Li, “Position-sensorless control technology of permanent-magnet synchronous motor-A review,” *Transactions of China Electrotechnical Society*, vol. 32, no. 16, pp. 76-88, Aug. 2017.

[4] S. Neethu, P. N. Saurabh, S. Sumeet, P. Saumitra, K. W. Ashok, and B. G. Fernandes, “High-speed coreless axial-flux permanent-magnet motor with printed circuit board winding,” *IEEE Transactions on Industry Applications*, vol. 55, no. 2, pp. 1954-1962, Mar-Apr. 2019.

[5] A. Athavale, K. Sasaki, B. S. Gagas, T. Kato, and R. D. Lorenz, “Variable flux permanent magnet synchronous machine (VF-PMSM) design methodologies to meet electric vehicle traction requirements with reduced losses,” *IEEE Transactions on Industry Applications*, vol. 53, no. 5, Sep-Oct. 2017.

[6] *Handbook of Magnetic Measurements*, ver. 1, Mechanical Industry Press, Beijing, BJ, 2014.

[7] A. H. Guo and J. M. Fu, “Measurement technology of magnetic flux and its application,” *Journal of Transducer Technology*, vol. 19, no. 4, pp. 1-4, Mar. 2000.

[8] D. M. Miles, B. B. Narod, D. K. Milling, I. R. Mann, and D. Barona, “A hybrid fluxgate and search coil magnetometer concept using a racetrack core,” *Geoscientific Instrumentation & Methods and Data Systems*, vol. 7, no. 4, pp. 265-276, Oct. 2018.

[9] N. Murata, H. Karo, I. Sasada, and T. Shimizu, “Fundamental mode orthogonal fluxgate magnetometer applicable for measurements of DC and low-frequency magnetic fields,” *IEEE Sensors Journal*, vol. 18, no. 7, pp. 2705-2712, Apr. 2018.

[10] Z. Q. Chu, H. D. Shi, M. J. PourhosseiniAsl, J. E. Wu, W. L. Shi, X. Y. Gao, X. T. Yuan, and S. X. Dong, “A magnetoelectric flux gate: new approach for weak DC magnetic field detection,” *Scientific Reports*, vol. 7, no. 1, pp. 8592, Aug. 2017.

[11] M. F. Snoeij, V. Schaffer, S. Udayashankar, and M. V. Ivanov, “Integrated fluxgate magnetometer for use in isolated current sensing,|” *IEEE Journal of Solid-State Circuits*, vol. 51, no. 7, pp. 1684-1694, May. 2016.

[12] A. F. Morabito, L. D. Donato, and T. Isernia, “Orbital angular momentum antennas: Understanding actual possibilities through the aperture antennas theory,” *IEEE Antennas and Propagation Magazine*, vol. 60, no. 2, pp. 59-67, Feb. 2018.

Xianming Deng was born in Sichuan, China. He received his B.S., M.S., and Ph.D. in Electrical Engineering from China University of Mining and Technology, Jiangsu, China. He is currently a Professor in the School of Electrical and Power Engineering of China University of Mining and Technology. His current research fields include power electronics and motor drive.

Junhong Zhou was born in Hunan, China. He received his B.S. in Information Engineering from China University of Mining and Technology, Jiangsu, China. He is currently receiving a Master education at China University of Mining and Technology. His current research interests include power electronics and motor drive.

Lei Hao was born in Shandong, China. He received his B.S. in Electrical Engineering from Shandong University of Technology, Shandong, China. He is currently receiving a Master education at China University of Mining and Technology. His current research interests include power electronics and motor drive.

Zhihua Fan was born in Shanghai, China. He received the B.S. degree in Electrical Engineering from Nanjing Institute of Technology, Jiangsu, China. He is currently receiving a Master education at China University of Mining and Technology. His current research interests include power electronics and motor drive.

Na Liu was born in Anhui, China. She received her B.S. and M.S. in Electrical Engineering from China University of Mining and Technology, Jiangsu, China. She is currently a Hardware Engineer at Institute of Electronics, Chinese Academy of Science. Her current research interests include power electronics and motor drive.